dips in the plots indicate resonant coupling of light into the waveguide and, by power conservation, out of the transmitted beam. While the vertical axis units are arbitrary, the absolute ratio of maximum to minimum transmission is greater than 50%. It was observed that the width of the lower-wavelength set of peaks is greater than that of the longer-wavelength peaks, as was argued in.[4,5]

The transmittance approaches 100% for angles and wavelengths which do not excite resonances in the waveguide. On resonance, light is coupled into the guide, is absorbed or scattered in other directions, and the observed intensity in the transmitted direction decreases rapidly. Key to the present work is the fact that, in a grating whose first-order component couples perpendicularly incident light into the guide, the second Bragg resonance of the same grating forms a stopband to propagation within the guide. The result is that, as normal incidence is approached, an anomalous spectral/angular dependence is observed. This is illustrated in figure 2. As we approach perpendicular incidence, the two dips in the transmittance spectrum move closer together, since forward and backward coupling become degenerate at this point. However, they do not completely merge, a fact attributed to the presence of the stopband in the grating for these wavelengths.

3. Conclusions

We have explored grating-assisted coupling of light into a waveguide formed using an optical interferometric technique deployed in an integrable, low-cost materials platform. Realization of both waveguide and the grating in polymers is conductive to photonic integrated circuit realization. Furthermore, since these gratings couple light almost perpendicularly incident onto the waveguide, they may be useful in coupling of light between different layers of circuits.

4. References

1. P. Rochon, E. Batalla and A. Natansohn, "Optically induced surface gratings on azoaromatic polymer films," Appl. Phys. Lett., **66** (1995).
2. D.Y. Kim, S.K. Tripathy, L. Lian and J. Kumar, "Laser-induced holographic surface relief gratings on nonlinear optical polymer films," Appl. Phys. Lett., **66** (1995).
3. R. Stockermans and P. Rochon, "Narrow-band resonant grating waveguide filters constructed with azobenzene polymers," Appl. Optics, **38** (1999).
4. I.A. Avrutskii, G.A. Golubenko, V.A. Sychugov and A.V. Tishchenko, "Spectral and laser characteristics of a mirror with a corrugated waveguide on its surface," Sov. J. Quantum. Electron, **16** (1986).
5. I.A. Avrutsky and V.A. Sychugov, "Reflection of a beam of finite size from a corrugated waveguide," J. Mod. Opt., **36** (1989).

CMS

3:45 pm–5:30 pm
Room: 324–326

High Speed Photonic Sampling and Switching

Thomas R. Clark, *Sowilo Networks, Inc., USA, Presider*

CMS1 **3:45 pm**

Mode-locked erbium/ytterbium co-doped waveguide laser

J.B. Schlager, B.E. Callicoatt, K.L. Silverman, R.P. Mirin, N.A. Sanford, D.L. Veasey,* *National Institute of Standards and Technology, 325 Broadway, Boulder, Colorado 80305; Email: schlager@boulder.nist.gov; *Yafo Networks, 1340 F Charwood Road, Hanover, MD 21076*

High-power, low-jitter optical pulse sources are critical for high-data-rate communication systems and optical sampling systems used for high-speed analog-to-digital conversion.[1] Planar waveguide lasers based on Er/Yb co-doped phosphate glass can produce continuous-wave output powers that exceed 170 mW.[2] These same lasers have the potential for producing similarly high average powers when mode locked. We present mode locking results using Er/Yb co-doped glass and semiconductor saturable absorber mirrors (SESAMs) that demonstrate improvements in output power over earlier work.[3] A typical laser configuration is shown in Fig. 1. Through coupling optics, a Ti:Sapphire laser pumps a 2 cm long waveguide positioned at one end of the laser cavity. The waveguide is fabricated in Er/Yb co-doped phosphate glass.[4] A partially reflecting mirror is butted to one facet of the waveguide with index-matching fluid and serves as an output coupler. The other facet is cut and polished at Brewster's angle to minimize intracavity reflections in the extended cavity setup. A microscope objective collimates the light from the waveguide, and this beam is focused down onto the SESAM with a second lens. Focal lengths for this lens range from 6.24 mm to 25.4 mm. Cavity lengths range from 40 cm to 2 m. Turning mirrors minimize the space required for the laser and reduce the intensity of the pump light that reaches the SESAM. A dichroic beamsplitter passes the 977 nm pump light and couples the 1534 nm laser output into an optical fiber.

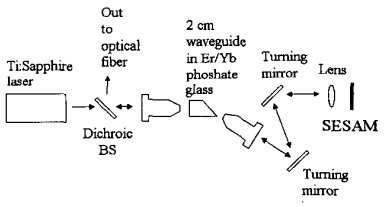

CMS1 Fig. 1. Extended-cavity mode-locked laser with 2 cm Er/Yb co-doped waveguide amplifier and SESAM mode locker.

Figure 2 shows the nonlinear reflectivity of the SESAM as a function of pulse fluence. An ultrafast optical parametric oscillator was used to collect these data at the SESAM peak reflectivity of 1540 nm. SESAMs were grown by molecular beam epitaxy. Three low-temperature InGaAs quantum wells with anti-resonant GaAs spacers serve as the fast saturable absorber; they sit atop a 22.5 period distributed Bragg reflector made from alternating quarter-wave layers of GaAs and AlAs. The absorber has a saturable loss ΔR of 9.5% ± 0.5%, a nonsaturable loss ($1 - R_{ns}$) of 3% ± 0.5%, and a saturation fluence F_{sat} of 25 $\mu J/cm^2$.

The pulsed output from a 2.2 m laser with a 10% output coupler is shown in Fig. 3. Here, the lens at the SESAM had a focal length of 25.4 mm. This provided about 50 $\mu J/cm^2$ of fluence on the SESAM with 240 mW of coupled pump power at 977 nm. Measured pulse durations were limited

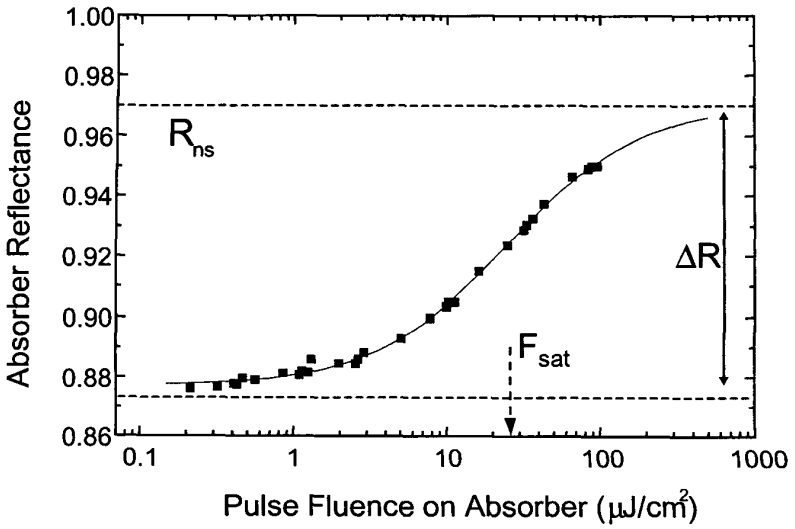

CMS1 Fig. 2. Semiconductor saturable absorber mirror reflectance (data and fit) as a function of pulse fluence on absorber with 150 fs pulses at 1540 nm.

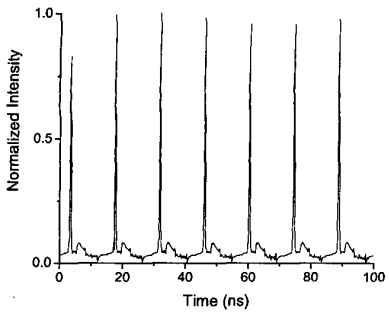

CMS1 Fig. 3. Pulsed output from a 2.2 m laser with a 10% output coupler and 240 mW of coupled pump power at 977 nm.

by the 25 ps response time of our sampling oscilloscope. Actual pulse durations are estimated to be shorter than 10 ps. Similar output was achieved with other laser configurations. A 1.5 m cavity and a 6.2 mm focal-length lens at the SESAM (>1000 μJ/cm^2 of fluence) gave detection-limited, picosecond pulses with average output powers over 8 mW. Pulse trains for all configurations exhibited some relaxation-oscillation instabilities, as revealed by sidebands in the radio frequency spectrum. These relaxation oscillations are driven by fluctuations in the pump source and are not attributed to simultaneous mode locking and Q switching of the Er/Yb extended-cavity laser. Improvements are expected with refinements in the SESAM design and with laser diode pumping.

References

1. J.C. Twichell, R. Helkey, IEEE Photon. Technol. Lett. 12, 1237 (2000).
2. D.S. Funk, D.L. Veasey, P.M. Peters, N.A. Sanford, and N.H. Fontaine, in *Optical Fiber Communications Conference,* OSA Technical Digest (Optical Society of America, Washington DC, 1999), pp. 32–34, paper TuC5-1 (1999).
3. E.R. Thoen, E.M. Koontz, D.J. Jones, D. Barbier, F.X. Kartner, E.P. Ippen, and L.A. Kolodziejski, IEEE Photon. Technol. Lett. 12, 149 (2000).
4. D.L. Veasey, D.S. Funk, P.M. Peters, N.A. Sanford, G.E. Obarski, N. Fontaine, M. Young, A.P. Peskin, W. Liu, S.N. Houde-Walter, J.S. Hayden, Journal of Non-Crystalline Solids, 263 & 264, 369–381 (2000).

CMS2 **4:00 pm**

Dependence of ultra-low timing jitter on intra-cavity loss for modelocked semiconductor light sources

A. Braun, V. Khalfin, J. Abeles, C. DePriest,* E. Park,* P. Delfyett, Jr.,* *Sarnoff Corporation, 201 Washington Road, Princeton, NJ 08901; Email: abraun@sarnoff.com; *CREOL, University of Central Florida, 4000 Central Florida, Blvd., Orlando, FL 32816*

Introduction

The use of stable optical pulse-trains as sampling pulses may allow for accurate analog-to-digital conversion of wide-band RF signals. Specifically, 10 Gbps pulse trains with 10-fs of timing jitter could provide for 12-bit A/D conversion of 10-GHz signals. Modelocked semiconductor lasers may provide the needed sampling pulses for such an application.[1–3] In determining timing jitter, the phase noise is typically integrated at offset frequencies below 10 MHz[4,5] To be useful for such systems, however, characterization of the phase noise up to the roundtrip frequency may be needed. In this paper, comparative measurements of timing jitter (10-Hz to 10-MHz) of a modelocked semiconductor laser under gain and loss modulation is shown. Further, a numerical model incorporating spontaneous emission is developed which points toward low-frequency noise as the main source of jitter. Indications of total timing jitter (10 Hz–5 GHz) on the order of 40-fs is given.

Experiment

The laser system utilizes an angle-striped semiconductor optical amplifier (SOA) emitting at 1.55-μm aligned within an external cavity resonator. The active ridge is situated on a mesa defined by isolation channels, resulting in a capacitance of approximately 3 pF. By direct gain modulation using a 1.0 mm long SOA, modelocking through 4-GHz was readily achieved and up to 8-GHz was demonstrated. Modelocking via loss modulation was obtained by incorporating a 15-GHz $LiNbO_3$ intensity modulator intra-cavity while maintaining the SOA DC-biased. In this configuration, 10-GHz modelocking was achieved with a measured timing jitter of 30-fs (10-Hz to 10-MHz).

Comparison of the timing jitter (10-Hz to 10-MHz) under both gain and loss modulation was performed as a function of modelocking rate and cavity loss. The results are shown in Figure 1. Capacitance effects reduce the modulation efficiency at higher drive frequency. This appears to increase the timing jitter for the case of gain modulation.

Simulation

Besides these phase noise measurements, it is important to begin to understand the effect of high

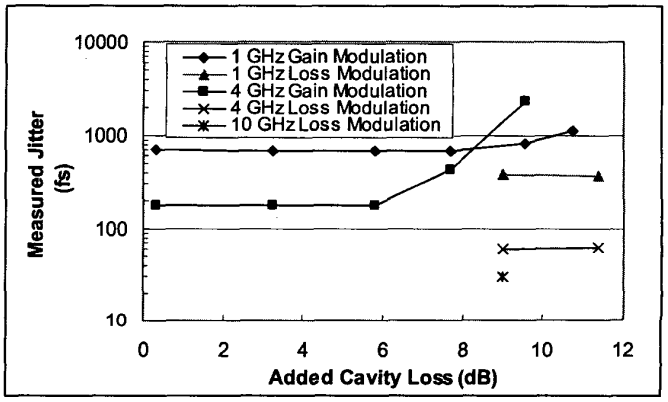

CMS2 Fig. 1. Measurement of timing jitter as a function of added cavity loss for both gain and loss modulation. Added loss is obtained from calibrated neutral-density filters. For loss-modulation, the intrinsic loss of modulator (9 dB) is included. Jitter is obtained from integrated phase noise (10 Hz-10 MHz). Capacitance limits the modulation efficiency resulting in an increased timing jitter for the case of gain modulation.

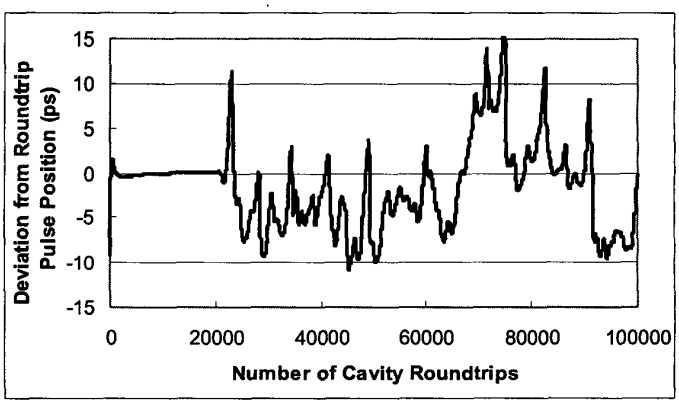

CMS2 Fig. 2. Simulation result of noise-driven pulse jitter represented as the deviation from initial round-trip pulse position. Cavity round trip time is 1 ns, the effective spontaneous emission factor is 10^{-5}, and the depth-of-modulation is 10%. The perturbation was implemented after 20,000 roundtrips to initially assure stable modelocking. Pulse-to-pulse jitter is on the order of 5-fs.